

Changes in satellite retrievals of atmospheric composition over eastern China during the 2020 COVID-19 lockdowns

Robert D. Field^{1,2}, Jonathan E. Hickman¹, Igor V. Geogdzhayev^{1,2}, Kostas Tsigaridis^{1,3}, Susanne E. Bauer¹

¹NASA Goddard Institute for Space Studies, 2880 Broadway, New York, NY, USA, 10025

²Dept. of Applied Physics and Applied Mathematics, Columbia University 2880 Broadway, New York, NY, USA, 10025

³Center for Climate Systems Research, Columbia University, 2880 Broadway, New York, NY, USA, 10025

Correspondence to: Robert D. Field (robert.field@columbia.edu)

Abstract. We examined daily Level-3 satellite retrievals of AIRS CO, OMI SO₂ and NO₂, and MODIS AOD over eastern China to understand how COVID-19 lockdowns affected atmospheric composition. Changes in 2020 were strongly dependent on the choice of background period since 2005 and whether trends in atmospheric composition were accounted for. Over central east China during the January 23 - April 8 lockdown window, CO in 2020 was between 3% and 12% lower than average depending on the background period, but not consistently less than expected from trends over different periods. Similarly for AOD, 2020 was between 14% and 30% lower than average, but not distinct from what would be expected from trends beginning after 2008. NO₂ in 2020 was between 30% and 43% lower than the mean over different background periods and between 17% and 33% lower than what would be expected for trends beginning later than 2011. Over southern China, 2020 NO₂ was between 23% and 32% lower than the mean, and between 14% and 29% lower than would be expected from different trends. CO over southern China was significantly higher than what would be expected, which we suggest was partly because of an active fire season in neighbouring countries. Over east central and southern China, SO₂ was higher than expected, but this depended strongly on how daily regional values were calculated from individual retrievals. Future work over China, or other regions, needs to take into account the sensitivity of differences in 2020 to different background periods and trends in order to separate the effects of COVID-19 on air quality from previously occurring changes, or from variability in other sources.

1 Introduction

In an effort to control the spread of COVID-19, the Chinese government implemented a range of restrictions on movement. These led to reductions in industrial and other work related and personal activities starting January 23, 2020 in Wuhan, Hubei province, then extending to other cities and regions in the days that followed. On April 8, 2020, Wuhan was the last city to re-open after a complete lockdown that prevented most people from leaving their homes. These measures have been linked to changes in air quality. A network of surface monitoring stations in northern China observed 35% decreases in PM_{2.5} and 60% decreases in NO₂ concentrations during January 29 through February 29, as compared to the preceding three weeks; CO and SO₂ also declined (Shi and Brasseur, 2020). In and around Wuhan, decreases of NO₂ and PM_{2.5} were similar to regional changes, but there was a slight increase in SO₂ concentrations (Shi and Brasseur, 2020). Observations by the Tropospheric Monitoring Instrument (TROPOMI) showed large decreases in tropospheric NO₂ column densities over Chinese cities, on the order of 40% for February 11 to March 24 2020 compared to the same period in 2019, ranging from roughly 25% for cities

39 not affected by lockdown to 60% for Wuhan and Xi'an (Bauwens et al., 2020). Prospective simulations suggested
40 that meteorology may limit the effect of reduced emissions on PM_{2.5} concentrations, with Chinese cities
41 experiencing less than 20% reductions (Wang et al., 2020).

42

43 The goal of our study was to consider these changes against pollution trends in China using NASA Earth
44 Observing System data by combining several products to give a holistic view covering several emission sectors
45 that are responsible for the observed changes. Over the last 2 to 3 decades, air pollution in China appears to have
46 followed the pattern described by the Environmental Kuznets Curve (Selden and Song, 1994). This framework
47 describes a relationship in which economic growth is initially accompanied by an increase in air pollution, when
48 poverty remains widespread. But as growth continues, air pollution is expected to level off and decline as a
49 consequence of changes in social awareness of environmental degradation and the economic, political, and
50 technological capacity to limit it (Sarkodie and Strezov, 2019;Selden and Song, 1994).

51

52 Bottom-up and top-down assessments of air pollutant emissions and concentrations suggest that China has
53 followed this pattern during the era of satellite monitoring of atmospheric composition, with concentrations of
54 SO₂, NO₂, CO, and aerosol optical depth (AOD) mostly exhibiting marked and steady declines over the last
55 decade. In the case of NO₂, multi-instrument analyses, which extend the observational record beyond the lifetime
56 of a single instrument, depict a consistent regional picture of NO₂ trends in China since 1996 (Geddes et al.,
57 2016;Georgoulias et al., 2019;Wang and Wang, 2020;Xu et al., 2020). Column totals show an increasing trend
58 during the first part of the satellite record, but this trend is reversed sometime between 2010 and 2014 (Georgoulias
59 et al., 2019;Krotkov et al., 2016;Lin et al., 2019;Xu et al., 2020;Si et al., 2019;Shah et al., 2020). The trend reversal
60 has been attributed to a combination of emission control measures (Zheng et al., 2018a) and variations in economic
61 growth (Krotkov et al., 2016).

62

63 Bottom-up estimates suggest that SO₂ emissions peaked earlier, with declines starting around 2005, primarily as
64 a result of power and industrial pollution control measures as well as the elimination of small industrial boilers
65 (Sun et al., 2018;Zheng et al., 2018b). An earlier peak in SO₂ emissions is consistent with observations by multiple
66 satellite instruments, which revealed declines in SO₂ column densities since 2005 (Fioletov et al., 2016;Krotkov
67 et al., 2016;Wang and Wang, 2020;Zhang et al., 2017;Si et al., 2019).

68

69 AOD retrievals from the Along Track Scanning Radiometer instruments show a steady increase over southeastern
70 China from 1995 to 2005 (Sogacheva et al., 2020), and a decline since 2005 in the MODIS AOD (He et al., 2019).
71 The AOD peak has been argued to match either the ~2011 peak in NO₂ (Zheng et al., 2018b;Xie et al., 2019), the
72 ~2005 peak of SO₂, or to have occurred at some point in between (Ma et al., 2016), with more rapid decreases in
73 AOD after 2011 (Lin et al., 2018). The recent decrease in AOD is also seen in VIIRS retrievals (Sogacheva et al.,
74 2020). Most mitigation of direct PM_{2.5} emissions since 2010 was by industry, with residential emissions also
75 decreasing substantially (Zheng et al., 2018b). The decline in SO₂ emissions also exerted an important influence,
76 with the sulfate concentration of PM_{2.5} decreasing substantially between 2013 and 2017 (Shao et al., 2018),
77 reflecting the negative trend in SO₂ emissions.

78

79 The peak in concentrations of CO, which has an atmospheric lifetime ranging from weeks to months, is less easily
80 identified. Some studies suggest that trends have been negative potentially throughout the 21st century (Han et al.,
81 2018;Strode et al., 2016;Wang et al., 2018;Yumimoto et al., 2014;Zheng et al., 2018a), but others suggest that
82 emissions and/or column densities were increasing or flat during at least the first decade of the century (Sun et
83 al., 2018;Zhao et al., 2013;Zhao et al., 2012). The negative trend has been attributed largely to reductions in
84 emissions from industrial activity, as well as from residential and transportation sectors (Zheng et al.,
85 2018a;Zheng et al., 2018b).

86

87 In addition to these long-term trends, a number of air pollutants also exhibit strong seasonal variation in China.
88 Anthropogenic emissions of CO, SO₂, and PM_{2.5} are highest in winter, reflecting large variation in emissions from
89 the residential sector and, in the case of CO, increased emissions associated with cold-start processes in the
90 transportation sector (Li et al., 2017). Outflow of CO and AOD has a spring maximum, resulting from transport
91 of pollution, dust, and boreal biomass burning emissions (Han et al., 2018;Luan and Jaegle, 2013).

92

93 Changes in pollution over China have also come from short-term interventions. To improve air quality for the
94 2008 summer Olympics—a time when emissions in China were high and still increasing—the Chinese
95 government imposed a series of strict emissions control measures from July through September 21, 2008, which
96 were qualitatively similar to the emissions reductions expected to have accompanied the COVID-19 lockdown
97 (UNEP, 2009). As a result, NO₂ concentrations over Beijing were estimated to have declined by between 40%
98 and 60% based on satellite observations, with substantial but smaller reductions in surrounding cities often on the
99 order of 20% to 30% compared to previous years (Mijling et al., 2009;Witte et al., 2009). Regional reductions of
100 SO₂ and CO during the months of the games were estimated to be 13% and 19%, respectively (Witte et al., 2009).
101 These results are broadly consistent with on-road observations (Wang et al., 2009), but larger than some surface
102 observations comparing concentrations before and after the emission control measures were implemented (Wang
103 et al., 2010).

104

105 The COVID-related lockdowns provide a similar natural experiment to the 2008 Beijing Olympics but on the
106 other side of the Kuznets curve. The fact that the lockdowns occurred during years of decreasing air pollution
107 needs to be taken into account in attributing changes in atmospheric composition to COVID-19 lockdowns,
108 independent of the long-term trend. Following Chen et al.'s (2020) analysis of air quality improvements on
109 mortality which controlled for changes in air quality since 2016, in this study we determine whether changes in
110 2020 in satellite retrievals of CO, SO₂, NO₂ and AOD departed significantly from the expected declines associated
111 with the long-term decreases in concentrations resulting from pollution controls and technological change.

112 **2 Data and methods**

113 We used daily Level-3 (L3) retrievals from four different instruments on three different NASA Earth Observing
114 System satellites. The Atmospheric Infrared Sounder (AIRS) instrument aboard NASA's Aqua satellite is a 2300-
115 channel infrared grating spectrometer in a sun-synchronous orbit with northward equator crossing time of 1:30
116 PM. AIRS carbon monoxide (CO) profiles are retrieved with horizontal resolution of 45 km at nadir, in a swath
117 of width 30 fields-of-view or about 1600 km. The retrieval uses a cloud-clearing methodology providing CO with

118 sensitivity that peaks around 500 hPa, with ~0.8-1.2 degrees-of-freedom-of-signal for 50-70% of scenes. More
119 sampling and higher information content is obtained in clear scenes (Warner et al., 2013). We used the daily
120 version 6 (AIRS3STD.006) product.

121

122 The Ozone Monitoring Instrument (OMI) aboard NASA's Aura satellite was launched in July 2004, and has a
123 local equator-crossing time of roughly 13:45. OMI is a nadir-viewing spectrometer, which measures solar
124 backscatter in the UV-visible range (Krotkov, 2013). We used NASA's L3 tropospheric NO₂ column density
125 Standard Product v3 (OMNO2d_003), and the OMI Principal Components Analysis Planetary Boundary Layer
126 (PBL) SO₂ product (OMSO2e_003), which grid retrievals to 0.25° resolution (Krotkov et al., 2017; Li et al., 2013).
127 Both products are cloud-screened; only pixels that are at least 70% cloud-free are included in the NO₂ product,
128 and those that are at least 80% cloud-free are included in the SO₂ product. The NO₂ product relies on air mass
129 factors (AMFs) calculated with the assistance of an atmospheric chemical transport model and are sensitive to
130 model representations of emission, chemistry, and transport data. Instead of AMFs, the SO₂ product uses
131 spectrally-dependent SO₂ Jacobians, but can be interpreted as having a fixed AMF that is representative of
132 summertime conditions. We applied basic transient SO₂ plume filtering, excluding retrievals with SO₂ > 15 DU
133 (Wang and Wang, 2020).

134

135 Because our trend analysis uses a seasonal mean as the response variable, we assume that random errors cancel
136 out, leaving only systematic errors, which do not contribute to uncertainty in the trend analysis. Systematic errors
137 in the OMI NO₂ product have an uncertainty of 20% (McLinden et al., 2014) and are associated with AMFs and
138 tropospheric vertical column contents. The OMI NO₂ products use an implicit aerosol correction to account for
139 the optical effects of aerosols, but retrievals can be biased when aerosol loading is extreme (Castellanos et al.,
140 2015). Under these conditions, the OMI NO₂ retrieval is biased low by roughly 20 to 40% (Chimot et al., 2016).
141 Note that any aerosol-related error would have the potential effect of underestimating the magnitude of decreases
142 in NO₂ column densities when comparing 2020 to previous years. Additional bias in the NO₂ product may be
143 introduced due to the reliance on nearly cloud-free pixels, in which greater sunlight may induce higher
144 photochemical rates. For example, the current NO₂ product is biased roughly 30% low over the Canadian oil sands
145 (McLinden et al., 2014). The level-2 OMI- NO₂ product has been validated against in situ and surface-based
146 observations showing good agreement (Lamsal et al., 2014). The use of fixed Jacobians in the SO₂ product
147 introduces systematic errors of 50 to 100% for cloud-free observations (Krotkov et al., 2016).

148

149 Starting in 2007, the quality of level 1B radiance data for some OMI viewing directions has been affected, known
150 as the row anomaly. The L3 products used here exclude all pixels affected by the row anomaly from each
151 observation, but the locations of the row anomaly pixels were dynamic between 2007 and 2011, which could
152 affect any comparisons including those years. Since 2011, the pixels affected by the row anomaly problem are the
153 same, so comparisons for data only since 2011 are not affected by changes in the row anomaly.

154

155 Moderate Resolution Imaging Spectroradiometer (MODIS) sensors observe the Earth from polar orbit, from Terra
156 satellite since 2000 and from Aqua since mid 2002. In this study we use MODIS-derived AOD at 550nm obtained
157 by merging Dark Target and Deep Blue retrievals (Sayer et al., 2014). Specifically, we use the

158 Deep_Blue_Aerosol_Optical_Depth_550_Land_Mean field over land and the over ocean
159 AOD_550_Dark_Target_Deep_Blue_Combined_Mean the from Collection 6.1 L3 Gridded products MYD08 and
160 MOD08 (Hubanks et al., 2019), though very few retrievals over ocean are included in our analysis. L3 values are
161 computed on $1^\circ \times 1^\circ$ spatial grid from L2 AOD products with resolution of 10x10 km. Over land 66% of MODIS-
162 retrieved Dark-target AOD values were shown to be $\pm 0.05 \pm 0.15 * \text{AOD}$ AERONET-observed values, with high
163 correlation ($R = 0.9$) (Levy et al., 2010). Around 78% of the Deep Blue retrievals are within the expected error
164 range of $\pm 0.05 \pm 0.20 * \text{AOD}$ (Sayer et al., 2013). MODIS AOD data have been extensively used by the modeling
165 and remote sensing scientific communities and inter-compared with a wide range of satellite AOD products (see
166 Schutgens et al. (2020) and references therein).

167

168 We analyzed these retrievals over two large regions (Fig. 1). Central east China was comprised of Shaanxi, Hubei,
169 Anhui, Jiangsu, Shanxi, Henan, Hebei, Shandong, Beijing, and Tianjin provinces. Southern China was comprised
170 of Guizhou, Guangxi, Hunan, Jiangxi, Guangdong, Fujian and Zhejiang provinces. Daily mean quantities were
171 calculated across all valid retrievals falling within the provinces comprising the regions. For the OMI NO₂
172 columns, individual retrievals were weighted by the L3 ‘Weight’ field, which is proportional to the fraction of the
173 grid cell with higher-quality retrievals, identified as those have less than 30% cloud fraction and not affected by
174 the row anomaly problem. We also calculated the daily value from the median of all retrievals, to understand
175 whether individual high values (mainly SO₂) had any effect on the significance of trends or differences between
176 2020 and different background periods. Monthly averages were calculated from the daily regional averages, with
177 each day weighted in the monthly average by the number of valid retrievals so as to not overrepresent days with
178 little satellite coverage or significant cloud cover. The monthly data were used to visually identify COVID-19
179 related changes against background seasonality and trends since 2005.

180

181 We examined the difference in the distribution of daily data during the 2020 January 23 to April 8 lockdown
182 period to the same period during previous years since 2005. We compared 2020 to 2019, to different background
183 periods, and to the expected value for 2020 estimated from trends over different background periods. We tested
184 the significance of these differences using bootstrap resampling (Efron and Gong, 1983) with a resampling size
185 of 2000. Given the uncertainty and uneven nature of trends over different parts of China from previous studies,
186 we identified the start of existing long-term trends for each species by conducting linear regressions of the change
187 in the four quantities over time for possible start years of 2005 to 2018. Each trend was estimated from the start
188 year in this range until 2019.

189

190 We also considered how the analysis depended on how the lockdown period was defined. Emissions and pollution
191 can decrease during the Chinese New Year holidays (Chen et al., 2020), which started as early as January 23 in
192 2012 and as late as February 19 in 2015, complicating COVID-19 related analyses of atmospheric composition
193 over China (Bauwens et al., 2020; Chen et al., 2020). The timing and extent of lockdowns also varied between
194 provinces and we assume that ‘slowdowns’ could have happened before or after stricter, official lockdowns. For
195 example, ground and air transportation remaining below lockdown levels nationally at least through April 14,
196 2020 (International Energy Agency, 2020). Excluding the holiday period from all years is a straightforward
197 approach to excluding any New Year holiday effects but will exclude simultaneous lockdown effects during the

198 initial, and presumably most strict, stages of the lockdown. Rather than specifying different combinations of New
199 Year holiday period and provincial-level lockdown timing, we used January 23-April 8 as our baseline period
200 (which will include all holiday periods since 2005), but examined the sensitivity of the statistics to the length of
201 the lockdown period, namely a longer lockdown period beginning one week earlier and one week later, and a
202 shorter lockdown period for February only. In interpreting the data, we put more confidence in 2020 differences
203 that were insensitive to these choices.

204 **3 Results**

205 **3.1 Regional patterns and seasonality**

206 Figure 2 shows the 2020 –2019 differences over China during the January 23-April 8 lockdown period for the
207 four satellite-retrieved quantities. There were decreases of 5-10 ppbv in AIRS CO over central east China (Fig.
208 2a) and increases of 20-25 ppbv over southern China in 2020 compared to 2019. The increase in southern China
209 is adjacent to a stronger positive CO anomaly over the upper Mekong regions of Myanmar, Thailand and Laos.
210 There were no coherent regional changes in OMI SO₂ (Fig. 2b), but rather smaller localized difference of either
211 sign. There were decreases in NO₂ (Fig. 2c) across central east China exceeding 8×10^{15} molec cm⁻² coincident
212 with the weaker decrease in CO. Over southern China, there were comparable differences over Guangdong
213 province, with smaller differences elsewhere. There was a decrease in MODIS AOD (Fig. 2d) in central-east
214 China coincident with the decreases in CO and NO₂, but smaller in magnitude. There was a region of higher AOD
215 in and northeast of the upper Mekong region coincident with the CO increase, both presumably because of biomass
216 burning.

217

218 To put the 2020/2019 difference maps in a longer-term and seasonal context, Figure 3 shows monthly averages
219 of the four retrieved quantities over central east China since 2005. There are seasonal CO peaks in March-April,
220 June and September, with the minima usually in November and December (Figure 3a). There has been a decrease
221 since 2005 in CO. The seasonal decrease from January to February in 2020 is similar to that which has occurred
222 occasionally before, but the CO during February and March 2020 was the lowest for that time of the year since
223 2005. By April, CO had returned to levels typical of 2015-2019. The main characteristics of the monthly SO₂ over
224 the region are that it has decreased since 2005 (Figure 3b), and that early 2020 SO₂ was within the range of recent
225 levels. There is a strong seasonal NO₂ cycle (Figure 3c), with a July-August minimum, and December-January
226 peak, which has been attributed to increased heating needs (Yu et al., 2017; Si et al., 2019) and longer chemical
227 lifetime owing to lower OH and RO₂ (Shah et al., 2020). NO₂ has also decreased since 2011, and during most
228 years, there is a departure from a smooth seasonal cycle in January and February associated with the Chinese New
229 Year holiday period. January and February 2020 NO₂ was considerably lower than previous years, increased
230 during March, and had recovered to typical, recent levels by April. AOD has consistent seasonal peaks in summer
231 which have been attributed to hygroscopic growth and agricultural residue burning (Filonchyk et al., 2019), but
232 had less regular seasonality otherwise, and has decreased since 2011. AOD during February and particularly
233 March of 2020 were lower than recent years, but during which time there was considerable variability in the
234 monthly data.

235

236 Figure 4 shows the four retrieved quantities over southern China. There is a springtime maximum in CO (Fig. 4a),
237 a less regular maximum during September-January, and an annual minimum in July. The range of CO is similar
238 to central east China. CO over the last 5 years is lower than earlier in the record, and early 2020 CO was higher
239 than recent years. SO₂ (Fig. 4b) is lower than central east China and any seasonal cycle is also hard to identify.
240 The high June 2011 values are due to the Nabro eruption in Ethiopia (Fromm et al., 2014) which is still apparent
241 in the time series despite excluding individual SO₂ retrievals that are greater than 15 DU, and are due to a
242 combination of higher overall background values and individual retrievals with very high (> 10 DU) SO₂. NO₂
243 (Fig. 4c) is lower than over east central China, but both regions share a similar seasonality. NO₂ during January-
244 April 2020 was slightly lower than in 2019. AOD (Fig. 4d) has weak seasonal peaks in October, March and June,
245 has decreased since 2011, and 2020 fell within the range of 2015-2019.
246

247 3.2 East central China

248 Figure 5 shows the CO, SO₂, NO₂ and AOD for January 23 – April 8 of each year over east central China as box
249 and whisker plots with the median, interquartile range and 2.5th and 97.5th percentiles over all daily mean data as
250 horizontal lines and the mean shown by the black dot. The associated statistics comparing 2020 and 2019 are
251 provided in Table 1, and comparing 2020 to longer background periods with and without trends accounted for as
252 supplementary Tables S1-S4. The AIRS CO is shown in Figure 5a. The variation during January 23 – April 8 of
253 each year is due to weather-related factors and observational error. The mean CO of 133.5 ppbv in 2020 was 3.2%
254 less than the 2019 mean of 137.9 ppbv, which was only marginally significant, having a 95% confidence interval
255 (-6.3% - 0.1%) close to spanning 0. During years prior, there were increases and decreases in CO from year to
256 year, but an overall decreasing trend since 2005. To quantify if the 2020 departure was significant against this
257 background, we compared the distribution of observed 2020 CO to the background average and to that which
258 might be expected given any trends over the background period. Because there was no obvious starting year for
259 the background period, we considered different periods starting in each year between 2005 and 2018 and ending
260 in 2019 (Fig. 6a, Table S1). The difference between 2020 and the background depended strongly on the starting
261 year of the background period, ranging from -11.5% lower than the 2005-2019 mean to -3.1% lower than over
262 2018-2019, but all were statistically significant. Significant trends over years beginning between 2005 and 2018
263 (shown in Fig. 6a by the red line and shading) ranged between -1.5 ppbv yr⁻¹ when starting in 2013 to -3.6 ppbv
264 yr⁻¹ if starting in 2016. The uncertainty in the trends increased for trends over shorter periods, and were,
265 unsurprisingly, insignificant by 2017, with the 95% confidence intervals of the trends spanning 0. The differences
266 between the observed 2020 mean and the value predicted from the trend (magenta line) varied inversely with the
267 trend and was always negative, but, except for 2009, had 95% confidence intervals (magenta shading) spanning
268 0, and therefore were not considered significant. For CO therefore, 2020 was significantly lower than the
269 background period mean but not consistently lower than predicted given the decreasing trend during the
270 background period, no matter how this period was defined. Results were similar for CO analysed closer to the
271 surface at 850 hPa (not shown), but where the retrieval has less sensitivity.
272

273 OMI SO₂ (Fig. 5b) fluctuated over 2005 to 2011 and declined steadily afterward during which variation also
274 declined, becoming narrower to a degree not seen in the CO. The 2020 mean of 0.057 was 95% higher than the

275 2019 mean of 0.031, but with a wide 95% confidence interval (15% - 250%). For different background periods
276 (Table S2), 2020 SO₂ ranged from 83% less than the 2005-2019 mean to 30% less than the 2016-2019 mean, with
277 insignificant differences compared to more recent periods. Trends varied significantly from to -0.03 yr⁻¹ over
278 2005-2019 to -0.06 DU yr⁻¹ over 2012-2019 (Fig. 6b), during which the trend could explain a maximum of 32%
279 of the variation in the data. For periods starting in 2007 and after, the observed 2020 mean was significantly higher
280 than predicted. Relative to the value predicted from the 2012-2019 trend of -0.06, the observed 2020 SO₂ was
281 200% higher; the large percent difference reflects a predicted value close to zero, and we note that the retrieved
282 SO₂ can be negative for individual values and averages (Li et al., 2013; Wang and Wang 2020). While this
283 difference was significant, the change in 2020 SO₂ was strongly dependent on whether daily values were
284 calculated from the mean or median of individual values over the region. For most background periods (Figure
285 S1b), the trends in the median values were still negative until 2015, but 2020 was only 8.4% higher than predicted
286 from the 2012-2019 trend and not significantly different from expected for trends beginning later. This likely
287 reflects the greater influence of high individual retrieval values on the daily mean value compared to the median,
288 even after the basic filtering of transient SO₂ plumes.

289
290 OMI NO₂ (Fig. 5c) increased from 2005 to 2011 and decreased thereafter with an apparent flattening since 2016.
291 The 2020 mean NO₂ of 6.5x10¹⁵ molec cm⁻² was 32% less than the 2019 mean of 9.6 x10¹⁵ molec cm⁻²; the
292 pronounced regional difference between 2020 and 2019 (Fig. 2c) in part reflects a 2019 uptick from 2018. For
293 different background periods (Table S3), 2020 NO₂ ranged from 43.3% less than the 2010-2019 mean to 30% less
294 than the 2018-2019 mean, with all differences significant. Trends were negative and significant for starting years
295 between 2007 and 2015 (Fig. 6c) with the strongest trend of -0.7 5x10¹⁵ molec cm⁻² yr⁻¹ for the period beginning
296 in 2011. 2020 NO₂ was significantly less than the predicted value for all background periods but varied from
297 16.8% less than predicted from the 2011-2019 trend to 27.1% less than predicted from the 2015-2019 trend, the
298 last period when there was a significant, although weak, decrease.

299
300 MODIS AOD (Fig. 5d) was flat or slightly increasing from 2005 to 2011, decreasing thereafter and with a
301 flattening since 2016 similar to SO₂ and NO₂. The 2020 mean AOD of 0.41 was 14% less than the 2019 mean of
302 0.48, but this was not significant. For different background periods (Table S4), 2020 AOD ranged from 30.2%
303 less than the 2007-2019 mean to 14.2% less than the 2018-2019 mean, confidence intervals for the differences
304 becoming closer to spanning 0 for more recent periods. Trends were negative and significant for starting years
305 between 2005 and 2014 (Fig. 6d), with the strongest decrease of 0.04 yr⁻¹ over the 2012-2019 period. There was
306 no significant difference between the observed and predicted 2020 mean for periods beginning in 2008 and later,
307 when the trends were strongest, and which approached 0 after 2014.

308 **3.3 Southern China**

309 Figure 7 shows the distribution of daily CO, SO₂, NO₂ and AOD for January 23-April 8 of each year over southern
310 China. The associated statistics comparing 2020 and 2019 are provided in Table 2. AIRS CO (Fig. 7a) in 2020
311 was 144.7 ppbv, 13% higher than the 2019 mean of 128.5 ppbv which can be seen in an upward shift in the
312 distribution of the box plot. 2020 CO was between 4.4% and 8.8% greater than the background mean for periods
313 starting after 2014 (Table S5), but not significantly different otherwise. CO decreased significantly for periods

314 starting between 2005 and 2016 (Fig. 8a). When these trends are taken into account, 2020 CO was between 11.2%
315 and 18.7% greater than predicted, and in all cases were significant.

316

317 OMI SO₂ (Fig. 7b) fluctuated from 2005 until 2013 and flattened afterwards, driven by fewer high individual SO₂
318 values in later years, as in east central China. The 2020 mean of 0.003 DU was 116% higher than the 2019 mean
319 of -0.02 DU but also with a wide 95% confidence interval (24% - 223%). 2020 was less than the background
320 mean periods starting between 2005 and 2011 (Table S6), but not significantly different otherwise. SO₂ trends
321 were consistently negative for all periods (Fig. 8b), although not as strong as over east central China. Whether
322 2020 SO₂ was greater than predicted from trends depended more on the background period than over east central
323 China and were also not significantly different from predicted when daily values were calculated from the median
324 SO₂ of individual retrievals for any background period (Figure S2b).

325

326 OMI NO₂ (Fig. 7c) increased toward 2011 and 2012, declining after to 2005-2010 levels. The 2020 mean of
327 3.3×10^{15} molec cm⁻² was 22% less than the 2019 mean of 4.3×10^{15} molec cm⁻². For longer background periods,
328 2020 was between 22.9% and 30.6% less than the mean (Table S7), all of which were significant. NO₂ trends
329 were significantly negative for periods beginning between 2007 and 2012, but not otherwise (Fig. 8c). The 2020
330 NO₂ mean was significantly lower than predicted, except for when the trend was estimated beginning in 2011 or
331 2018. A two-year trend is hard to interpret meaningfully, but visually, it is hard to tell if the 2020 NO₂ distribution
332 represents a COVID-related departure or a decrease comparable to changes during recent previous years, unlike
333 over central east China.

334

335 MODIS AOD (Fig. 7d) was comparable to NO₂ in its increase toward 2012, decrease thereafter and flattening
336 during more recent years. The 2020 mean AOD of 0.38 was 12% higher than the 2019 mean of 0.34, but with a
337 95% confidence interval (-7% - 34%) spanning 0. Similarly, 2020 was between 14% and 22% lower than during
338 background periods beginning from 2005 to 2012, but not for more recent periods (Table S8). The AOD trends
339 were significantly negative for all start years until 2015. The 2020 mean was between 32 and 47% higher than
340 predicted from trends for periods starting between 2010 and 2015, but not otherwise.

341

342 For both regions and all quantities, the differences between observed and predicted values for 2020 were
343 insensitive to a longer lockdown period, or to whether the bootstrap resampling was weighted by the number of
344 valid retrievals each day. For a February-only lockdown period (Figures S5 and S6), the CO trends were more
345 significant when starting in later years, but the differences between the observed and expected values for remained
346 insignificant. The SO₂ trends for different periods were similar. The 2020 SO₂ differences from what would be
347 expected approached 0 for later periods but were also inconsistent when the median values of individual
348 retrievals were used. Results for NO₂ were unaffected. The AOD 2020 difference from what would be expected
349 was stronger and technically significant, but still with a very wide confidence interval and therefore difficult to
350 interpret. We emphasize that while a February-only lockdown period is useful for comparison, it is problematic
351 in not including the New Year's holiday periods from all previous years.

352 4 Discussion and conclusions

353 The degree to which the COVID-19 lockdowns in China resulted in changes in atmospheric composition depended
354 strongly on the background period and whether existing trends were taken into account. For AIRS CO over central
355 east China, the 2020 mean was 12% less than that over 2005-2019 and 3% lower than since 2018, but was not
356 consistently different from what would be expected given the steady decreases over different periods. Similarly
357 for MODIS AOD, the 2020 mean was between 14% and 30% less than different background averages, but not
358 significantly different from what would be expected for trends beginning after 2008. 2020 SO₂ was significantly
359 lower than background averages calculated over most periods, ranging from 83% less than over 2005-2019 to
360 30% less than over 2016-2019. Compared to the 2012-2019 period when there were no significant SO₂ increases,
361 2020 SO₂ was 200% greater than what would be expected, but only 8% greater when the median value was used,
362 and not significantly different from expected relative to the trends beginning later than 2012. We note that analyses
363 of SO₂ and NO₂ that include years prior to 2012 may be affected by changes in observation sample size due to
364 changes in the OMI row anomaly.

365

366 OMI NO₂ in 2020 over central east China was consistently lower than the background average and expected value
367 from the trends, but the latter value ranged from 17% for a trend calculated over 2011-2019 to a 33% decrease
368 compared to 2018-2019 during which NO₂ trends had flattened. While there were clear decreases in 2020 NO₂,
369 this does suggest that some part of the reductions in NO₂ in 2020 could be expected independent of COVID-19
370 lockdowns. For reference, Bauwens et al. (2020) reported a ~40% drop in OMI NO₂ from 2019 to 2020 over cities
371 affected by the lockdown using the QA4ECV retrieval (Boersma et al., 2018), and a ~51% drop in NO₂ over the
372 eight cities (Beijing, Jinan, Nanjing, Qingdao, Tianjin, Wuhan, Xi'an and Zhengzhou) falling within our central
373 east China region. Our analysis cannot be compared directly because we include non-urban areas and define the
374 lockdown period differently, but we can say that some of the reduction in that study is possibly due to background
375 trends in addition to COVID-19 lockdowns.

376

377 The lack of any significant departure from recent trends in CO and AOD over central east China was unexpected,
378 given its high population density and level of industrial activity. In the case of MODIS AOD, the lack of an
379 observable lockdown effect was possibly due to contributions from other sources unaffected by COVID-19 related
380 lockdowns, limitations in the MODIS AOD retrieval under cloudy conditions, climatological variability from
381 other sources such as mineral dust, and meteorology favourable to secondary aerosol formation which could have
382 offset lower emissions (Wang et al., 2020). The 2020 increase in SO₂ is more difficult to interpret because of the
383 discrepancies between daily values calculated from the mean or median of individual retrievals, but is broadly
384 consistent with surface observations that find no significant change in in-situ surface SO₂ over Wuhan in the daily
385 mean, and a slight increase in daytime SO₂ possibly associated with increased residential heating and cooking
386 (Shi and Brasseur, 2020).

387

388 Over southern China, retrieved 2020 SO₂ was significantly lower than the background average only for periods
389 beginning between 2005 to 2011. Significant departures from expected trends uneven for the mean value and
390 absent for the median value. NO₂ in 2020 was between 23% and 32% less than the background average for
391 different periods, and between 14% and 23% less than expected from trends, with insignificant differences when

392 trends were calculated beginning in 2011 or 2018. The more significant reductions in NO₂ in east central China
393 compared to the south is presumably due the former's greater population and industrialization, and consequently
394 higher pollution levels. This is consistent with Chen et al.'s (2020) detection of a larger 2020 decrease in surface
395 NO₂ in Wuhan compared to Shanghai. Retrieved CO in 2020 was between 4 and 8% greater than background
396 averages beginning in 2014, but between 11% and 19% higher than what would be expected given the decreasing
397 trends over any period. AOD in 2020 was lower than background averages beginning until 2012, but higher or
398 not significantly different from expected for trends beginning after.

399

400 The focus of this analysis is on whether satellite retrievals of atmospheric composition over 2020 departed
401 significantly from different background periods and expected values for 2020 when daily variability and trends
402 are accounted for, but it is useful at a preliminary stage to speculate as to how different emissions changes could
403 have contributed to 1) why NO₂ was robustly lower in 2020 over east central China compared to CO and AOD,
404 and 2) why CO and perhaps AOD were higher over southern China compared to what would be expected from
405 recent trends.

406

407 To understand why NO₂ differences over east central China were more significant than other quantities, Table 3
408 shows the emissions by sector for a representative set of constituents from the Community Emissions Data System
409 (CEDS) (Hoesly et al., 2018) over China for 2014, the most recent year available. Other bottom-up emissions
410 inventories will vary in absolute emissions amounts and their sector contributions, particularly for more recent
411 periods, but CEDS is the standard available emissions dataset available globally as a baseline for the next IPCC
412 assessment, in anticipation of assessing 2020 COVID-19 related changes to atmospheric composition in other
413 regions, and for modeling studies involving a transboundary transport component. Across all species, energy
414 production, industrial activity, transportation, residential/commercial/other (RCO), and waste disposal constitute
415 the bulk of the emissions. Based on activity data for the first quarter of 2020, energy demand across China declined
416 by 7% compared to 2019, and transportation sector activity declined by 50 to 75% in regions with lockdowns in
417 place (International Energy Agency, 2020). These sectors are direct or indirect sources of numerous pollutants,
418 including SO₂ (the precursor of sulfate aerosol), NO_x, CO, and primary anthropogenic aerosols classified broadly
419 as organic carbon (OC) and black carbon (BC). If we apply the 7% reduction in energy production and mid-point
420 62.5% reduction to transportation from the IEA, assume a 20% reduction in industrial emissions, 5% reduction in
421 waste emissions, no change in RCO (with commercial decreases offset by residential increases), this yields a 10%
422 reduction in BC, 5% reduction in OC, 14% reduction in SO₂, 14% reduction in CO and 21% reduction in NO₂.
423 The larger reduction in NO₂ relative to other emissions could partly explain why OMI NO₂ column density
424 changes over central east China were stronger than in the other retrievals.

425

426 Following Si et al.'s (2019) consideration of biomass burning as a pollution source in China alongside
427 anthropogenic sources, we considered transboundary smoke transport as a possible reason for the higher 2020 CO
428 over southern China, guided by higher CO over the Upper Mekong region in 2020 compared to 2019 (Fig. 2a)
429 and the predominant westerly flow during this time of year (Reid et al., 2013). Table 4 compares January 23-April
430 8 AIRS CO over southern China to CO emissions estimates from biomass burning from the Global Fire
431 Assimilation System (GFAS) (Kaiser et al., 2012) over the upper Mekong region (17° N to 25° N, 95° E to 105°

432 E) including parts of eastern Myanmar, northern Thailand, and northern Laos. From 2005 to 2020, variation in
433 GFAS CO over this region explained a moderate (32%) amount of variability in AIRS CO over southern China,
434 suggesting it as a non-negligible contributor to variation in CO concentration, and a contributor to higher CO
435 in 2020. This illustrates that, at a minimum, sources such as biomass burning smoke and dust that are less affected
436 by COVID-19 related measures will complicate attribution studies. To that end, modeling studies following Wang
437 et al. (2020) will be required to isolate emissions, meteorological and chemical drivers of changes in atmospheric
438 composition and their effects at a process level. With proper instrument-equivalent comparisons, modelling
439 studies will also help to identify the extent to which the lack of significant changes are due to retrieval limitations,
440 namely low sensitivity near the surface where differences would presumably be more pronounced, particularly
441 given remote emissions sources such as dust, biomass burning smoke and volcanic SO₂, which will arrive at higher
442 altitudes.

443

444 The key implication of our study is that interpreting differences in 2020 retrievals of atmospheric composition
445 depends strongly on how the background period is defined and whether trends over these periods are accounted
446 for. Not taking these into account could lead to misattribution of changes in air quality to COVID-19 lockdowns,
447 or, at a minimum, that whether differences in 2020 are significant depend on the choice of background period,
448 which is somewhat subjective. We have approached the issue by comparing data for 2020 to what would have
449 been expected given recent trends and by applying a single lockdown period to two large regions, with additional
450 analyses to gauge the sensitivity of the 2020 differences to these choices. Other studies over China or elsewhere
451 will inevitably use other approaches that more explicitly account for seasonality, meteorology, and which relate
452 changes in pollution over smaller areas (e.g. single provinces or states) to region-specific lockdown measures and
453 timing at a process level. Regardless of the approach, however, it is important to consider recent trends and
454 variability. In places where pollution has decreased, not accounting for recent context could result in over-
455 attribution of changes in pollution to COVID-19. In places where pollution has increased, such as parts of South
456 Asia, this could result in under-attribution.

457 **Code/data availability:** All code will be made available if the article is accepted for final publication. All source
458 data are publicly available.

459

460 **Competing interests:** The authors have no competing interests.

461

462 **Author contribution:** All authors conceived of the study. RF, IG and KT conducted the data analysis. RF and
463 JH prepared the manuscript with contributions from all co-authors.

464

465 **References**

- 466 Bauwens, M., Compernelle, S., Stavrakou, T., Müller, J., van Gent, J., Eskes, H., Levelt, P. F., van der A., R.,
467 Veeffkind, J. P., Vlietinck, J., Yu, H., and Zehner, C.: Impact of coronavirus outbreak on NO₂ pollution assessed using
468 TROPOMI and OMI observations, *Geophysical Research Letters*, 2, 0-3, 10.1029/2020GL087978, 2020.
- 469 Boersma, K. F., Eskes, H. J., Richter, A., De Smedt, I., Lorente, A., Beirle, S., van Geffen, J., Zara, M., Peters, E.,
470 Van Roozendael, M., Wagner, T., Maasakkers, J. D., van der A., R. J., Nightingale, J., De Rudder, A., Irie, H., Pinardi,
471 G., Lambert, J. C., and Compernelle, S. C.: Improving algorithms and uncertainty estimates for satellite NO₂
472 retrievals: results from the quality assurance for the essential climate variables (QA4ECV) project, *Atmospheric*
473 *Measurement Techniques*, 11, 6651-6678, 10.5194/amt-11-6651-2018, 2018.
- 474 Castellanos, P., Boersma, K. F., Torres, O., and de Haan, J. F.: OMI tropospheric NO₂ air mass factors over South
475 America: effects of biomass burning aerosols, *Atmospheric Measurement Techniques*, 8, 3831-3849, 10.5194/amt-8-
476 3831-2015, 2015.
- 477 Chen, K., Wang, M., Huang, C., Kinney, P. L., and Paul, A. T.: Air Pollution Reduction and Mortality Benefit during
478 the COVID-19 Outbreak in China, *Lancet Planetary Health*, 0-3, 10.1101/2020.03.23.20039842, 2020.
- 479 Chimot, J., Vlemmix, T., Veeffkind, J. P., de Haan, J. F., and Levelt, P. F.: Impact of aerosols on the OMI tropospheric
480 NO₂ retrievals over industrialized regions: how accurate is the aerosol correction of cloud-free scenes via a simple
481 cloud model?, *Atmospheric Measurement Techniques*, 9, 359-382, 10.5194/amt-9-359-2016, 2016.
- 482 Efron, B., and Gong, G.: A Leisurely Look at the Bootstrap, the Jackknife, and Cross-Validation, *American Statistician*,
483 37, 36-48, 10.2307/2685844, 1983.
- 484 Filonchyk, M., Yan, H. W., and Zhang, Z. R.: Analysis of spatial and temporal variability of aerosol optical depth
485 over China using MODIS combined Dark Target and Deep Blue product, *Theoretical and Applied Climatology*, 137,
486 2271-2288, 10.1007/s00704-018-2737-5, 2019.
- 487 Fioletov, V. E., McLinden, C. A., Krotkov, N., Li, C., Joiner, J., Theys, N., Carn, S., and Moran, M. D.: A global
488 catalogue of large SO₂ sources and emissions derived from the Ozone Monitoring Instrument, *Atmospheric Chemistry*
489 *and Physics*, 16, 11497-11519, 10.5194/acp-16-11497-2016, 2016.
- 490 Fromm, M., Kablick, G., Nedoluha, G., Carboni, E., Grainger, R., Campbell, J., and Lewis, J.: Correcting the record
491 of volcanic stratospheric aerosol impact: Nabro and Sarychev Peak, *Journal of Geophysical Research-Atmospheres*,
492 119, 10.1002/2014jd021507, 2014.
- 493 Geddes, J. A., Martin, R. V., Boys, B. L., and van Donkelaar, A.: Long-Term Trends Worldwide in Ambient NO₂
494 Concentrations Inferred from Satellite Observations, *Environmental Health Perspectives*, 124, 281-289,
495 10.1289/ehp.1409567, 2016.
- 496 Georgoulias, A. K., van der A., R. J., Stammes, P., Boersma, K. F., & Eskes, H. J.: Trends and trend reversal detection
497 in two decades of tropospheric NO₂ satellite observations, *Atmospheric Chemistry and Physics*, 19, 6269–6294,
498 <https://doi.org/10.5194/acp-2018-988>, 2019.
- 499 Han, H., Liu, J., Yuan, H. L., Jiang, F., Zhu, Y., Wu, Y., Wang, T. J., and Zhuang, B. L.: Impacts of Synoptic Weather
500 Patterns and their Persistency on Free Tropospheric Carbon Monoxide Concentrations and Outflow in Eastern China,
501 *Journal of Geophysical Research-Atmospheres*, 123, 7024-7046, 10.1029/2017jd028172, 2018.

- 502 He, Q. Q., Gu, Y. F., and Zhang, M.: Spatiotemporal patterns of aerosol optical depth throughout China from 2003 to
503 2016, *Science of the Total Environment*, 653, 23-35, 10.1016/j.scitotenv.2018.10.307, 2019.
- 504 Hoesly, R. M., Smith, S. J., Feng, L. Y., Klimont, Z., Janssens-Maenhout, G., Pitkanen, T., Seibert, J. J., Vu, L.,
505 Andres, R. J., Bolt, R. M., Bond, T. C., Dawidowski, L., Kholod, N., Kurokawa, J., Li, M., Liu, L., Lu, Z. F., Moura,
506 M. C. P., O'Rourke, P. R., and Zhang, Q.: Historical (1750-2014) anthropogenic emissions of reactive gases and
507 aerosols from the Community Emissions Data System (CEDS), *Geoscientific Model Development*, 11, 369-408,
508 10.5194/gmd-11-369-2018, 2018.
- 509 Hubanks, P., Platnick, S., King, M., and Ridgway, B.: MODIS Algorithm Theoretical Basis Document No. ATBD-
510 MOD-30 for Level-3 Global Gridded Atmosphere Products (08_D3, 08_E3, 08_M3) and Users Guide (Collection 6.0
511 & 6.1, Version 4.4, 20 Feb 2019), NASA Goddard Space Flight Center, Greenbelt, MD, 2019.
- 512 Kaiser, J. W., Heil, A., Andreae, M. O., Benedetti, A., Chubarova, N., Jones, L., Morcrette, J. J., Razinger, M., Schultz,
513 M. G., Suttie, M., and van der Werf, G. R.: Biomass burning emissions estimated with a global fire assimilation system
514 based on observed fire radiative power, *Biogeosciences*, 9, 527-554, 10.5194/bg-9-527-2012, 2012.
- 515 Krotkov, N. A.: OMI/Aura NO₂ Cloud-Screened Total and Tropospheric Column L3 Global Gridded 0.25 degree x
516 0.25 degree V3, NASA Goddard Space Flight Center, 2013.
- 517 Krotkov, N. A., McLinden, C. A., Li, C., Lamsal, L. N., Celarier, E. A., Marchenko, S. V., Swartz, W. H., Bucsela,
518 E. J., Joiner, J., Duncan, B. N., Boersma, K. F., Veefkind, J. P., Levelt, P. F., Fioletov, V. E., Dickerson, R. R., He,
519 H., Lu, Z., and Streets, D. G.: Aura OMI observations of regional SO₂ and NO₂ pollution changes from 2005 to 2015,
520 *Atmospheric Chemistry and Physics*, 16, 4605-4629, 10.5194/acp-16-4605-2016, 2016.
- 521 Krotkov, N. A., Lamsal, L. N., Celarier, E. A., Swartz, W. H., Marchenko, S. V., Bucsela, E. J., Chan, K. L., Wenig,
522 M., and Zara, M.: The version 3 OMI NO₂ standard product, *Atmospheric Measurement Techniques*, 10, 3133-3149,
523 10.5194/amt-10-3133-2017, 2017.
- 524 Lamsal, L. N., Krotkov, N. A., Celarier, E. A., Swartz, W. H., Pickering, K. E., Bucsela, E. J., Gleason, J. F., Martin,
525 R. V., Philip, S., Irie, H., Cede, A., Herman, J., Weinheimer, A., Szykman, J. J., and Knepp, T. N.: Evaluation of OMI
526 operational standard NO₂ column retrievals using in situ and surface-based NO₂ observations, *Atmospheric
527 Chemistry and Physics*, 14, 11587-11609, 10.5194/acp-14-11587-2014, 2014.
- 528 Levy, R. C., Remer, L. A., Kleidman, R. G., Mattoo, S., Ichoku, C., Kahn, R., and Eck, T. F.: Global evaluation of
529 the Collection 5 MODIS dark-target aerosol products over land, *Atmospheric Chemistry and Physics*, 10, 10399-
530 10420, 10.5194/acp-10-10399-2010, 2010.
- 531 Li, C., Joiner, J., Krotkov, N. A., and Bhartia, P. K.: A fast and sensitive new satellite SO₂ retrieval algorithm based
532 on principal component analysis: Application to the ozone monitoring instrument, *Geophysical Research Letters*, 40,
533 6314-6318, 10.1002/2013gl058134, 2013.
- 534 Li, M., Zhang, Q., Kurokawa, J., Woo, J. H., He, K. B., Lu, Z. F., Ohara, T., Song, Y., Streets, D. G., Carmichael, G.
535 R., Cheng, Y. F., Hong, C. P., Huo, H., Jiang, X. J., Kang, S. C., Liu, F., Su, H., and Zheng, B.: MIX: a mosaic Asian
536 anthropogenic emission inventory under the international collaboration framework of the MICS-Asia and HTAP,
537 *Atmospheric Chemistry and Physics*, 17, 935-963, 10.5194/acp-17-935-2017, 2017.
- 538 Lin, C. Q., Liu, G., Lau, A. K. H., Li, Y., Li, C. C., Fung, J. C. H., and Lao, X. Q.: High-resolution satellite remote
539 sensing of provincial PM 2.5 trends in China from 2001 to 2015. *Atmospheric Environment*, 180, 110-116,
540 <https://doi.org/10.1016/j.atmosenv.2018.02.045>, 2018.
- 541 Lin, N., Wang, Y. X., Zhang, Y., and Yang, K.: A large decline of tropospheric NO₂ in China observed from space
542 by SNPP OMPS, *Science of the Total Environment*, 675, 337-342, 10.1016/j.scitotenv.2019.04.090, 2019.

- 543 Luan, Y., and Jaegle, L.: Composite study of aerosol export events from East Asia and North America, *Atmospheric*
544 *Chemistry and Physics*, 13, 1221-1242, 10.5194/acp-13-1221-2013, 2013.
- 545 Ma, Z. W., Hu, X. F., Sayer, A. M., Levy, R., Zhang, Q., Xue, Y. G., Tong, S. L., Bi, J., Huang, L., and Liu, Y.:
546 *Satellite-Based Spatiotemporal Trends in PM_{2.5} Concentrations: China, 2004-2013*, *Environmental Health*
547 *Perspectives*, 124, 184-192, 10.1289/ehp.1409481, 2016.
- 548 McLinden, C. A., Fioletov, V., Boersma, K. F., Kharol, S. K., Krotkov, N., Lamsal, L., Makar, P. A., Martin, R. V.,
549 Veefkind, J. P., and Yang, K.: Improved satellite retrievals of NO₂ and SO₂ over the Canadian oil sands and
550 comparisons with surface measurements, *Atmospheric Chemistry and Physics*, 14, 3637-3656, 10.5194/acp-14-3637-
551 2014, 2014.
- 552 Mijling, B., van der A, R. J., Boersma, K. F., Van Roozendaal, M., De Smedt, I., and Kelder, H. M.: Reductions of
553 NO₂ detected from space during the 2008 Beijing Olympic Games, *Geophysical Research Letters*, 36,
554 10.1029/2009gl038943, 2009.
- 555 Reid, J. S., Hyer, E. J., Johnson, R. S., Holben, B. N., Yokelson, R. J., Zhang, J. L., Campbell, J. R., Christopher, S. A., Di
556 Girolamo, L., Giglio, L., Holz, R. E., Kearney, C., Miettinen, J., Reid, E. A., Turk, F. J., Wang, J., Xian, P., Zhao, G. Y.,
557 Balasubramanian, R., Chew, B. N., Janjai, S., Lagrosas, N., Lestari, P., Lin, N. H., Mahmud, M., Nguyen, A. X., Norris, B.,
558 Oanh, N. T. K., Oo, M., Salinas, S. V., Welton, E. J., and Liew, S. C.: Observing and understanding the Southeast Asian
559 aerosol system by remote sensing: An initial review and analysis for the Seven Southeast Asian Studies (7SEAS) program,
560 *Atmospheric Research*, 122, 403-468, 10.1016/j.atmosres.2012.06.005, 2013.
- 561
562 Sarkodie, S. A., and Strezov, V.: A review on Environmental Kuznets Curve hypothesis using bibliometric and meta-
563 analysis, *Science of the Total Environment*, 649, 128-145, 10.1016/j.scitotenv.2018.08.276, 2019.
- 564 Sayer, A. M., Hsu, N. C., Bettenhausen, C., and Jeong, M. J.: Validation and uncertainty estimates for MODIS
565 Collection 6 "Deep Blue" aerosol data, *Journal of Geophysical Research-Atmospheres*, 118, 7864-7872,
566 10.1002/jgrd.50600, 2013.
- 567 Sayer, A. M., Munchak, L. A., Hsu, N. C., Levy, R. C., Bettenhausen, C., and Jeong, M. J.: MODIS Collection 6
568 aerosol products: Comparison between Aqua's e-Deep Blue, Dark Target, and "merged" data sets, and usage
569 recommendations, *Journal of Geophysical Research-Atmospheres*, 119, 13965-13989, 10.1002/2014jd022453, 2014.
- 570 Schutgens, N., Sayer, A. M., Heckel, A., Hsu, C., Jethva, H., de Leeuw, G., Leonard, P. J. T., Levy, R. C., Lipponen,
571 A., Lyapustin, A., North, P., Popp, T., Poulson, C., Sawyer, V., Sogacheva, L., Thomas, G., Torres, O., Wang, Y.,
572 Kinne, S., Schulz, M., and Stier, P.: An AeroCom/AeroSat study: Intercomparison of Satellite AOD Datasets for
573 Aerosol Model Evaluation, *Atmos. Chem. Phys. Discuss.*, 2020, 1-43, 10.5194/acp-2019-1193, 2020.
- 574 Selden, T. M., and Song, D. Q.: Environmental Quality and Development - is there a Kuznets Curve for Air-Pollution
575 Emissions?, *Journal of Environmental Economics and Management*, 27, 147-162, 10.1006/jeem.1994.1031, 1994.
- 576 Shah, V., Jacob, D. J., Li, K., Silvern, R. F., Zhai, S. X., Liu, M. Y., Lin, J. T., and Zhang, Q.: Effect of changing NO_x
577 lifetime on the seasonality and long-term trends of satellite-observed tropospheric NO₂ columns over China,
578 *Atmospheric Chemistry and Physics*, 20, 1483-1495, 10.5194/acp-20-1483-2020, 2020.
- 579 Shao, P. Y., Tian, H. Z., Sun, Y. J., Liu, H. J., Wu, B. B., Liu, S. H., Liu, X. Y., Wu, Y. M., Liang, W. Z., Wang, Y.,
580 Gao, J. J., Xue, Y. F., Bai, X. X., Liu, W., Lin, S. M., and Hu, G. Z.: Characterizing remarkable changes of severe
581 haze events and chemical compositions in multi-size airborne particles (PM₁, PM_{2.5} and PM₁₀) from January 2013
582 to 2016-2017 winter in Beijing, China, *Atmospheric Environment*, 189, 133-144, 10.1016/j.atmosenv.2018.06.038,
583 2018.

- 584 Shi, X., and Brasseur, G. P.: The Response in Air Quality to the Reduction of Chinese Economic Activities during the
585 COVID-19 Outbreak, *Geophysical Research Letters*, 0-1, 10.1029/2020GL088070, 2020.
- 586 Si, Y. D., Wang, H. M., Cai, K., Chen, L. F., Zhou, Z. C., and Li, S. S.: Long-term (2006-2015) variations and relations
587 of multiple atmospheric pollutants based on multi-remote sensing data over the North China Plain, *Environmental*
588 *Pollution*, 255, 10.1016/j.envpol.2019.113323, 2019.
- 589 Sogacheva, L., Popp, T., Sayer, A. M., Dubovik, O., Garay, M. J., Heckel, A., Hsu, N. C., Jethva, H., Kahn, R. A.,
590 Kolmonen, P., Kosmale, M., de Leeuw, G., Levy, R. C., Litvinov, P., Lyapustin, A., North, P., Torres, O., and Arola,
591 A.: Merging regional and global aerosol optical depth records from major available satellite products, *Atmospheric*
592 *Chemistry and Physics*, 20, 2031-2056, 10.5194/acp-20-2031-2020, 2020.
- 593 Strode, S. A., Worden, H. M., Damon, M., Douglass, A. R., Duncan, B. N., Emmons, L. K., Lamarque, J.-F., Manyin,
594 M., Oman, L. D., Rodriguez, J. M., Strahan, S. E., and Tilmes, S.: Interpreting space-based trends in carbon monoxide
595 with multiple models, *Atmospheric Chemistry and Physics*, 16, 7285-7294, 10.5194/acp-16-7285-2016, 2016.
- 596 Sun, W., Shao, M., Granier, C., Liu, Y., Ye, C. S., and Zheng, J. Y.: Long-Term Trends of Anthropogenic SO₂, NO_x,
597 CO, and NMVOCs Emissions in China, *Earth's Future*, 6, 1112-1133, 10.1029/2018ef000822, 2018.
- 598 United Nations Environment Program (UNEP): Independent Environmental Assessment: Beijing 2008 Olympic
599 Games. Nairobi, Kenya, 2009.
- 600 Wang, M., Zhu, T., Zheng, J., Zhang, R. Y., Zhang, S. Q., Xie, X. X., Han, Y. Q., and Li, Y.: Use of a mobile laboratory
601 to evaluate changes in on-road air pollutants during the Beijing 2008 Summer Olympics, *Atmospheric Chemistry and*
602 *Physics*, 9, 8247-8263, 10.5194/acp-9-8247-2009, 2009.
- 603 Wang, P., Chen, K., Zhu, S., Wang, P., and Zhang, H.: Severe air pollution events not avoided by reduced
604 anthropogenic activities during COVID-19 outbreak, *Resources, Conservation and Recycling*, 158, 104814,
605 10.1016/j.resconrec.2020.104814, 2020.
- 606 Wang, P. C., Elansky, N. F., Timofeev, Y. M., Wang, G. C., Golitsyn, G. S., Makarova, M. V., Rakitin, V. S., Shtabkin,
607 Y., Skorokhod, A. I., Grechko, E. I., Fokeeva, E. V., Safronov, A. N., Ran, L., and Wang, T.: Long-Term Trends of
608 Carbon Monoxide Total Columnar Amount in Urban Areas and Background Regions: Ground- and Satellite-based
609 Spectroscopic Measurements, *Advances in Atmospheric Sciences*, 35, 785-795, 10.1007/s00376-017-6327-8, 2018.
- 610 Wang, T., Nie, W., Gao, J., Xue, L. K., Gao, X. M., Wang, X. F., Qiu, J., Poon, C. N., Meinardi, S., Blake, D., Wang,
611 S. L., Ding, A. J., Chai, F. H., Zhang, Q. Z., and Wang, W. X.: Air quality during the 2008 Beijing Olympics:
612 secondary pollutants and regional impact, *Atmospheric Chemistry and Physics*, 10, 7603-7615, 10.5194/acp-10-7603-
613 2010, 2010.
- 614 Wang, Y., and Wang, J.: Tropospheric SO₂ and NO₂ in 2012-2018: Contrasting views of two sensors (OMI and
615 OMPS) from space, *Atmospheric Environment*, 223, 10.1016/j.atmosenv.2019.117214, 2020.
- 616 Warner, J., Carminati, F., Wei, Z., Lahoz, W., and Attie, J. L.: Tropospheric carbon monoxide variability from AIRS
617 under clear and cloudy conditions, *Atmospheric Chemistry and Physics*, 13, 12469-12479, 10.5194/acp-13-12469-
618 2013, 2013.
- 619 Witte, J. C., Schoeberl, M. R., Douglass, A. R., Gleason, J. F., Krotkov, N. A., Gille, J. C., Pickering, K. E., and
620 Livesey, N.: Satellite observations of changes in air quality during the 2008 Beijing Olympics and Paralympics,
621 *Geophysical Research Letters*, 36, 10.1029/2009gl039236, 2009.

622 Xie, G. Q., Wang, M., Pan, J., and Zhu, Y.: Spatio-temporal variations and trends of MODIS C6.1 Dark Target and
623 Deep Blue merged aerosol optical depth over China during 2000-2017, *Atmospheric Environment*, 214,
624 10.1016/j.atmosenv.2019.116846, 2019.

625 Xu, J. H., Xie, H. M., Wang, K., Wang, J., and Xia, Z. S.: Analyzing the spatial and temporal variations in tropospheric
626 NO₂ column concentrations over China using multisource satellite remote sensing, *Journal of Applied Remote
627 Sensing*, 14, 10.1117/1.jrs.14.014519, 2020.

628 Yu, S. M., Yuan, J. G., and Liang, X. Y.: Trends and Spatiotemporal Patterns of Tropospheric NO₂ over China During
629 2005-2014, *Water Air and Soil Pollution*, 228, 10.1007/s11270-017-3641-9, 2017.

630 Yumimoto, K., Uno, I., and Itahashi, S.: Long-term inverse modeling of Chinese CO emission from satellite
631 observations, *Environmental Pollution*, 195, 308-318, 10.1016/j.envpol.2014.07.026, 2014.

632 Zhang, Y., Li, C., Krotkov, N. A., Joiner, J., Fioletov, V., and McLinden, C.: Continuation of long-term global SO₂
633 pollution monitoring from OMI to OMPS, *Atmospheric Measurement Techniques*, 10, 10.5194/amt-10-1495-2017,
634 2017.

635 Zhao, Y., Nielsen, C. P., McElroy, M. B., Zhang, L., and Zhang, J.: CO emissions in China: Uncertainties and
636 implications of improved energy efficiency and emission control, *Atmospheric Environment*, 49, 103-113,
637 10.1016/j.atmosenv.2011.12.015, 2012.

638 Zhao, Y., Zhang, J., and Nielsen, C. P.: The effects of recent control policies on trends in emissions of anthropogenic
639 atmospheric pollutants and CO₂ in China, *Atmospheric Chemistry and Physics*, 13, 487-508, 10.5194/acp-13-487-
640 2013, 2013.

641 Zheng, B., Chevallier, F., Ciais, P., Yin, Y., Deeter, M. N., Worden, H. M., Wang, Y. L., Zhang, Q., and He, K. B.:
642 Rapid decline in carbon monoxide emissions and export from East Asia between years 2005 and 2016, *Environmental
643 Research Letters*, 13, 10.1088/1748-9326/aab2b3, 2018a.

644 Zheng, B., Tong, D., Li, M., Liu, F., Hong, C. P., Geng, G. N., Li, H. Y., Li, X., Peng, L. Q., Qi, J., Yan, L., Zhang,
645 Y. X., Zhao, H. Y., Zheng, Y. X., He, K. B., and Zhang, Q.: Trends in China's anthropogenic emissions since 2010 as
646 the consequence of clean air actions, *Atmospheric Chemistry and Physics*, 18, 14095-14111, 10.5194/acp-18-14095-
647 2018, 2018b.

648

649 **Tables**

650

651 **Table 1. Summary statistics for central east China comparing 2020 and 2019 during January 23 – April 8.**

Variable	2020 mean	2019 mean	2020 % difference from 2019
CO (ppbv)	133.5 (130.3, 136.8)	137.9 (134.7, 141.3)	-3.2 (-6.3, 0.1)
SO₂ (DU)	0.057 (0.045, 0.070)	0.031 (0.018, 0.046)	95 (14.8, 249.6)
NO₂ (10 ¹⁵ molec cm ⁻²)	6.5 (5.8, 7.2)	9.6 (8.7, 10.5)	-32.1 (-42.1, -21.7)
AOD	0.41 (0.36, 0.46)	0.48 (0.41, 0.55)	-14.3 (-29.4, 3.1)

652

653

654 **Table 2. Same as Table 1, but for southern China.**

Variable	2020 mean	2019 mean	2020 % difference from 2019
CO (ppbv)	144.7 (139.6, 150.3)	128.5 (124.4, 132.8)	12.6 (7.2, 18.3)
SO₂ (DU)	0.003 (-0.01, 0.020)	-0.020 (-0.04, -0.001)	116 (24, 223)
NO₂ (10 ¹⁵ molec cm ⁻²)	3.3 (3.0, 3.7)	4.3 (3.9, 4.7)	-22.2 (-32.6, -10.4)
AOD	0.38 (0.34, 0.43)	0.34 (0.30, 0.39)	12 (-7, 34)

655

656 **Table 3. 2014 anthropogenic emissions estimates by sector (in %) over China, excluding biomass burning, from the**
657 **Community Emissions Data System (CEDs) for a representative set of constituents: black carbon (BC), carbon monoxide**
658 **(CO), ammonia (NH₃), nitrogen oxides (NO_x), organic carbon (OC) and sulfur dioxide (SO₂). Residential, commercial and**
659 **other sectors are combined as RCO.**

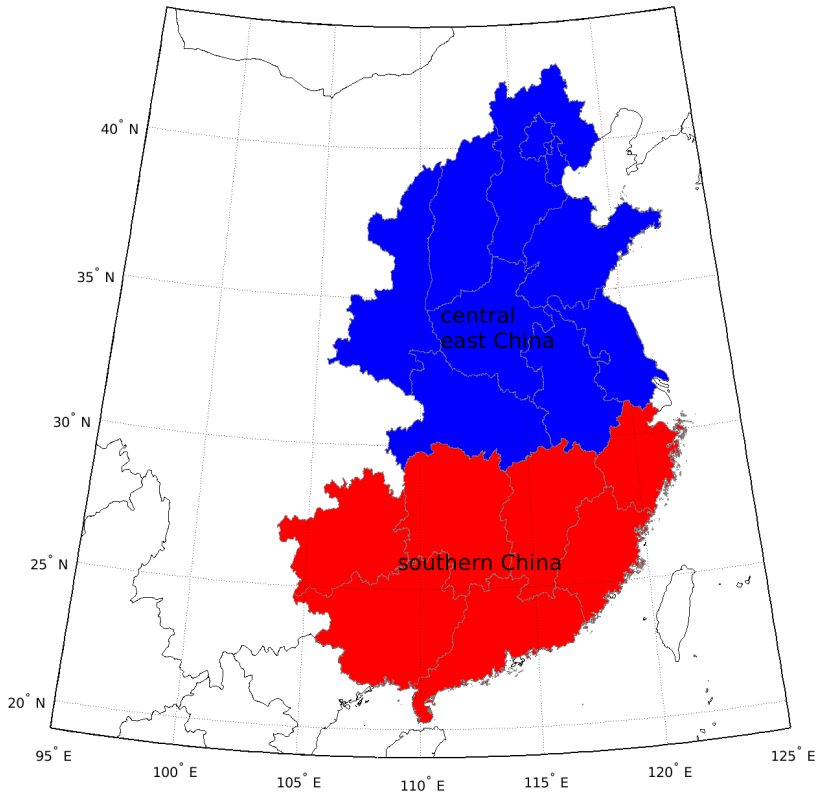
	BC	CO	NH₃	NO_x	OC	SO₂
Agriculture	0	0	61.6	1.1	0	0
Energy	32.6	8	0.4	38.5	28.3	29.4
Industrial	12.7	41.8	6.5	33	5.1	57.3
Ground transportation	8.1	7.2	0.5	17.5	1.7	0.3
RCO	38.1	36.7	5.2	4.2	38.4	12.5
Solvents	0	0	0	0	0	0
Waste	8.5	6.3	25.8	5.2	26.5	0.4
Shipping	0	0	0	0.2	0	0.1
Aircraft	0	0	0	0.2	0	0

660

661 **Table 4. Bottom up biomass Global Fire Assimilation System (Kaiser et al., 2012) burning CO emissions estimates from the**
 662 **Upper Mekong region (17° N to 24° N, 95° E to 105° E) and AIRS CO over southern China from January 23 to April 8, for**
 663 **2005-2020.**

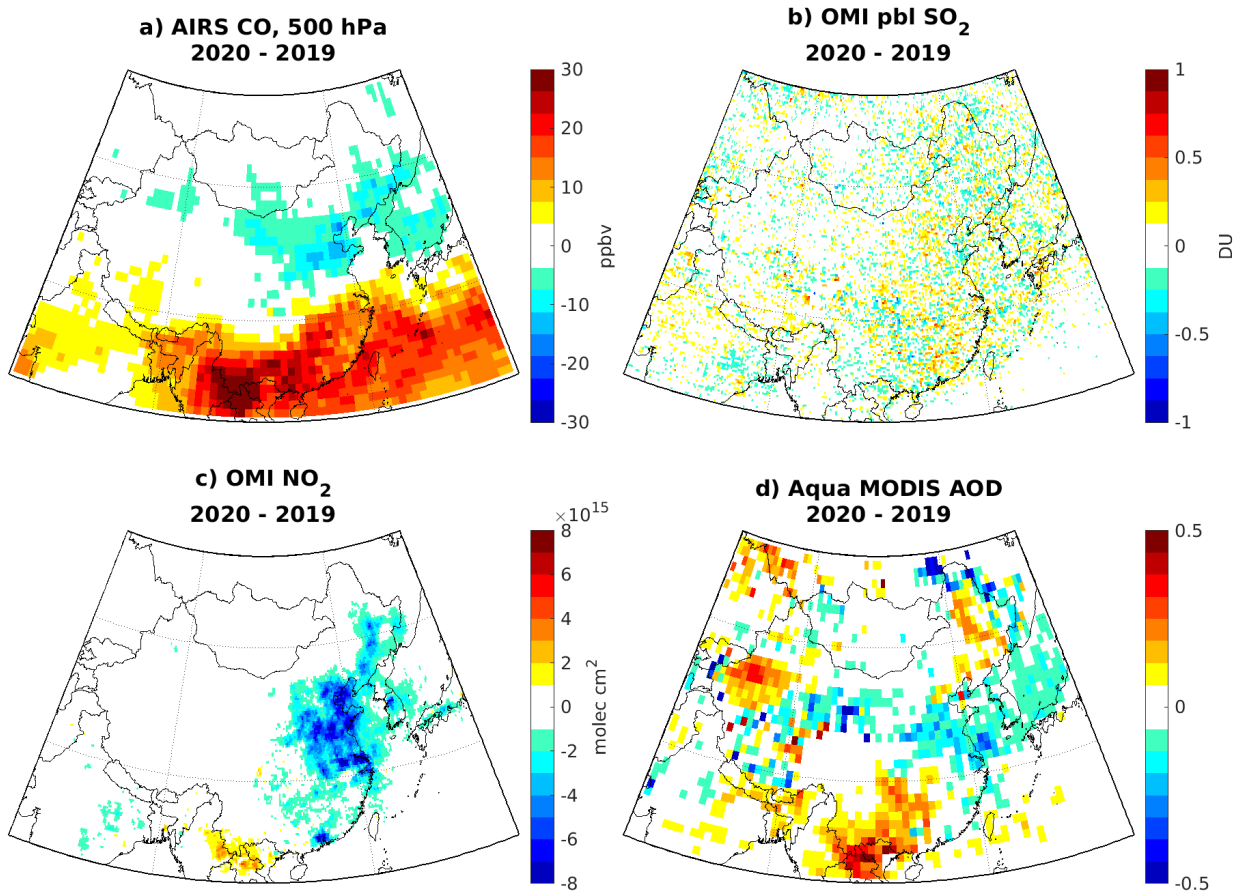
Year	GFAS CO	AIRS CO
	Upper Mekong (KT)	southern China 500 hPa (ppbv)
2005	7977	157
2006	8905	146
2007	15734	165
2008	4542	153
2009	9990	140
2010	14176	149
2011	3591	147
2012	11320	153
2013	8684	145
2014	8722	142
2015	8084	143
2016	9642	149
2017	3736	131
2018	3179	139
2019	6309	128
2020	7871	145

664



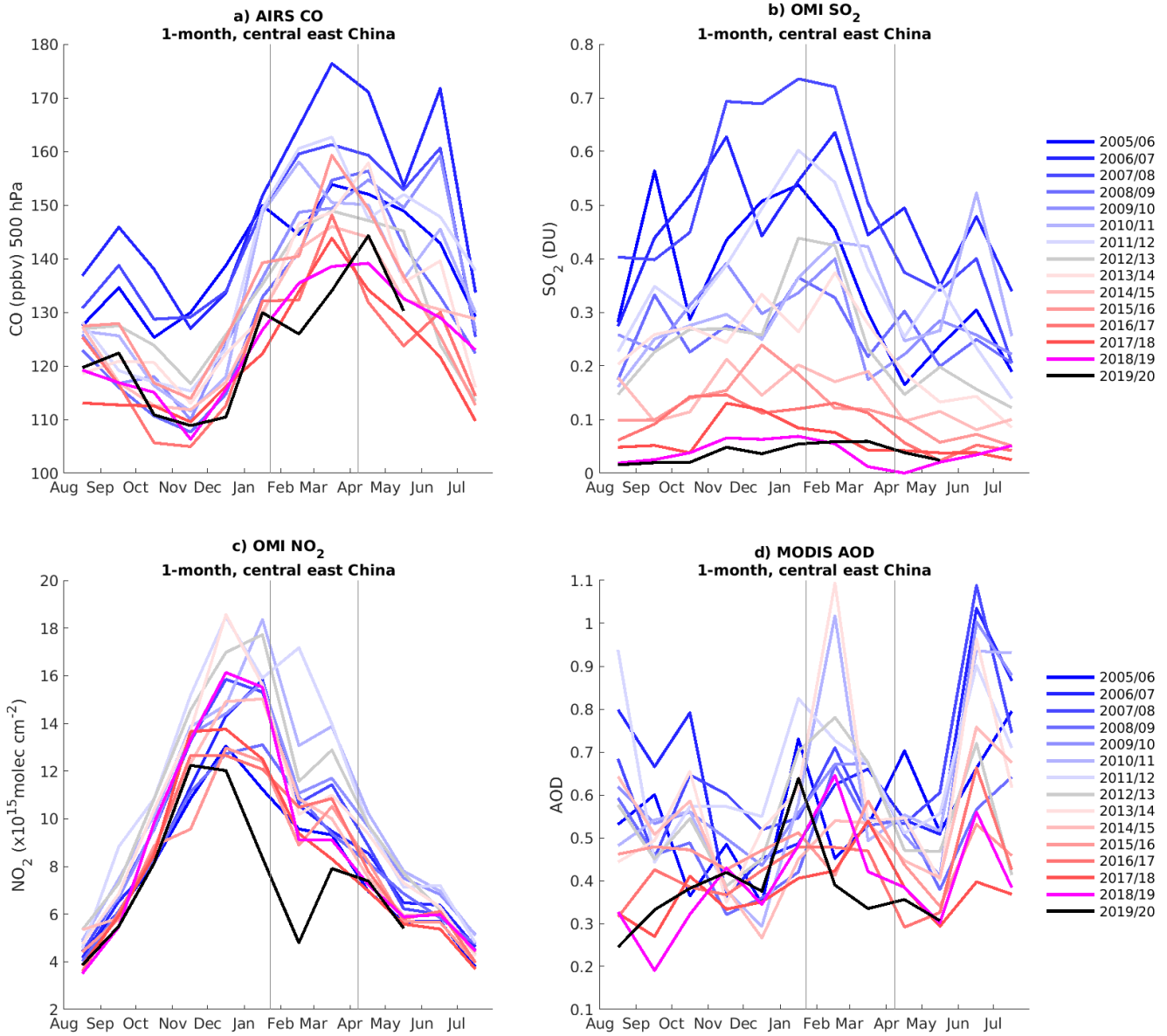
666

667 **Figure 1. Groupings of provinces for central east China and southern China.**



668

669 **Figure 2. 2020-2019 differences during January 23 to April 8 over China in a) AIRS carbon monoxide (CO) at 500 hPa, b)**
 670 **OMI PBL sulfur dioxide (SO₂), c) OMI tropospheric nitrogen dioxide (NO₂) and d) Aqua MODIS aerosol optical depth**
 671 **(AOD).**



675 **Figure 3. Monthly mean a) AIRS CO, b) OMI PBL SO₂, c) OMI tropospheric NO₂ and d) MODIS AOD over central east China since 2005. As in Bauwens et al. (2020), each year starts in August to show any departure from the seasonal cycle during the January 23 to April 8 lockdown period, shown by the thin grey vertical lines.**

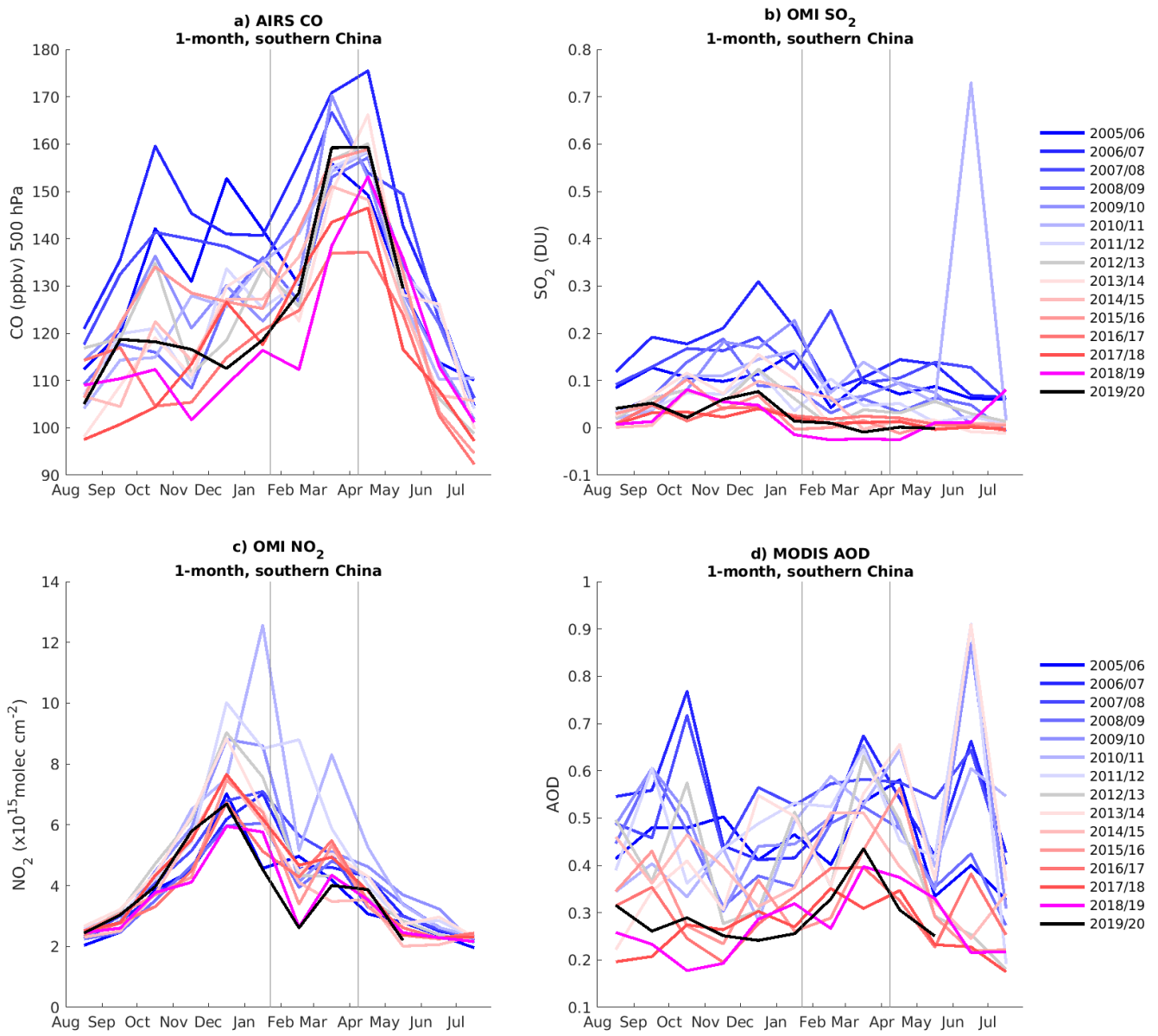
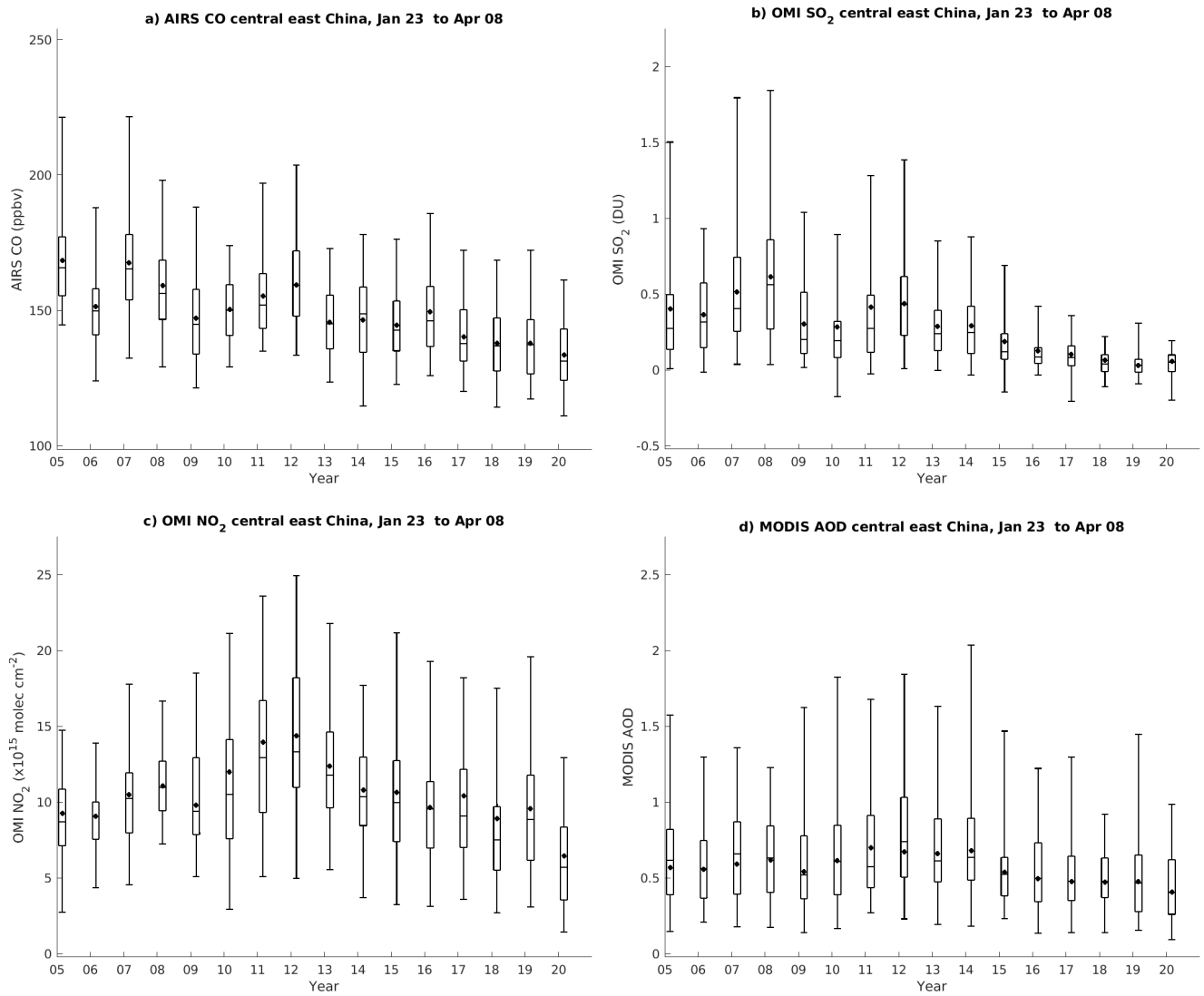
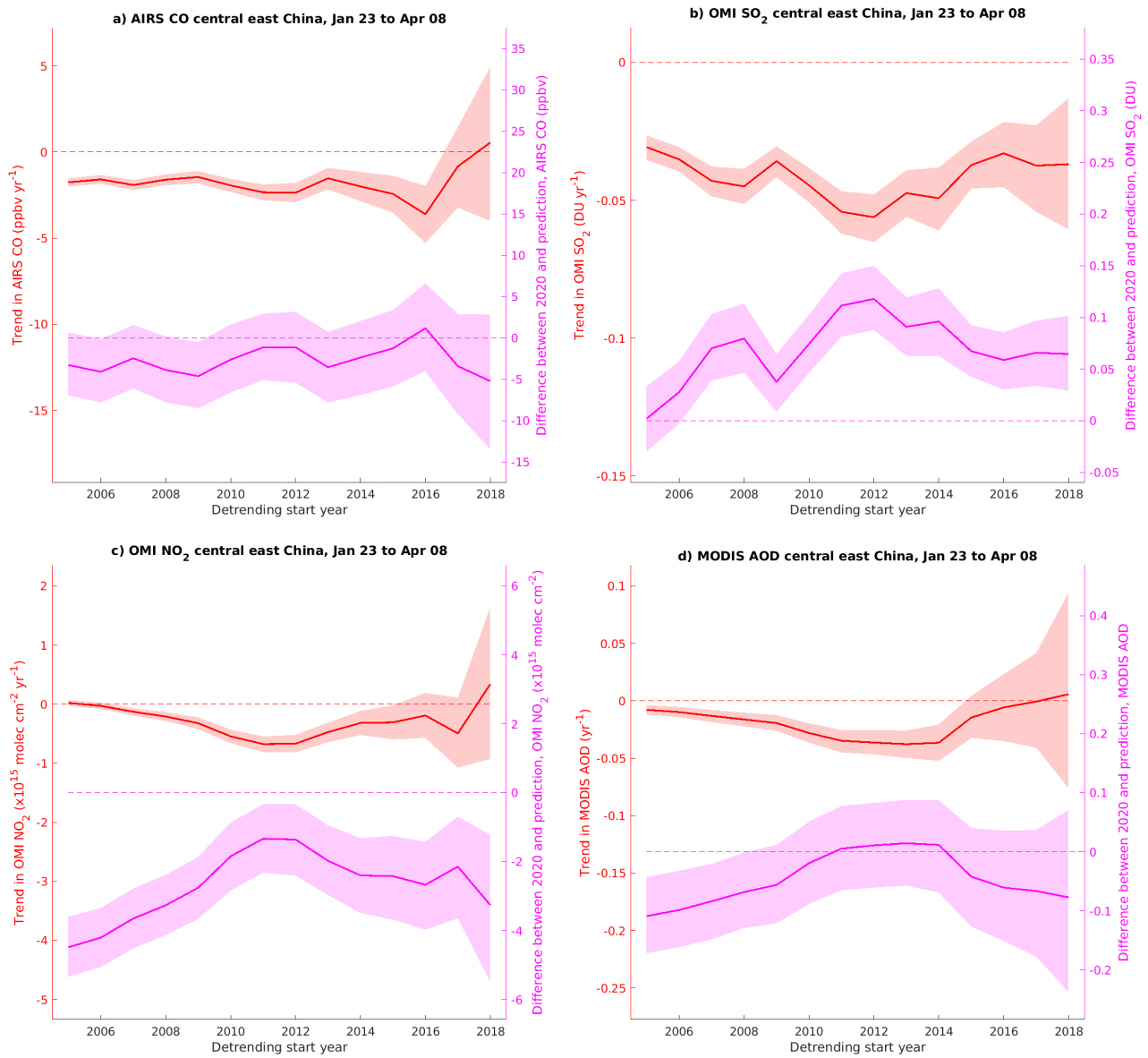


Figure 4. Same as Figure 3, but for southern China.



680 **Figure 5. January 23-April 8 box plots over central East China for a) AIRS CO, b) OMI PBL SO₂, c) OMI tropospheric NO₂ and d) Aqua and Terra MODIS AOD from 2005 to 2020. The black box plots show the median, interquartile range and 2.5th and 97.5th percentiles over all daily data, with the mean shown by the black dot.**



685 **Figure 6. Dependence of trends (red) and difference between 2020 observations and predicted value (magenta) on detrending start year over central east China for a) AIRS CO, b) OMI PBL SO₂, c) OMI tropospheric NO₂ and d) MODIS AOD. The solid line shows the mean of the estimate for each year and the shading shows the 95% confidence interval.**

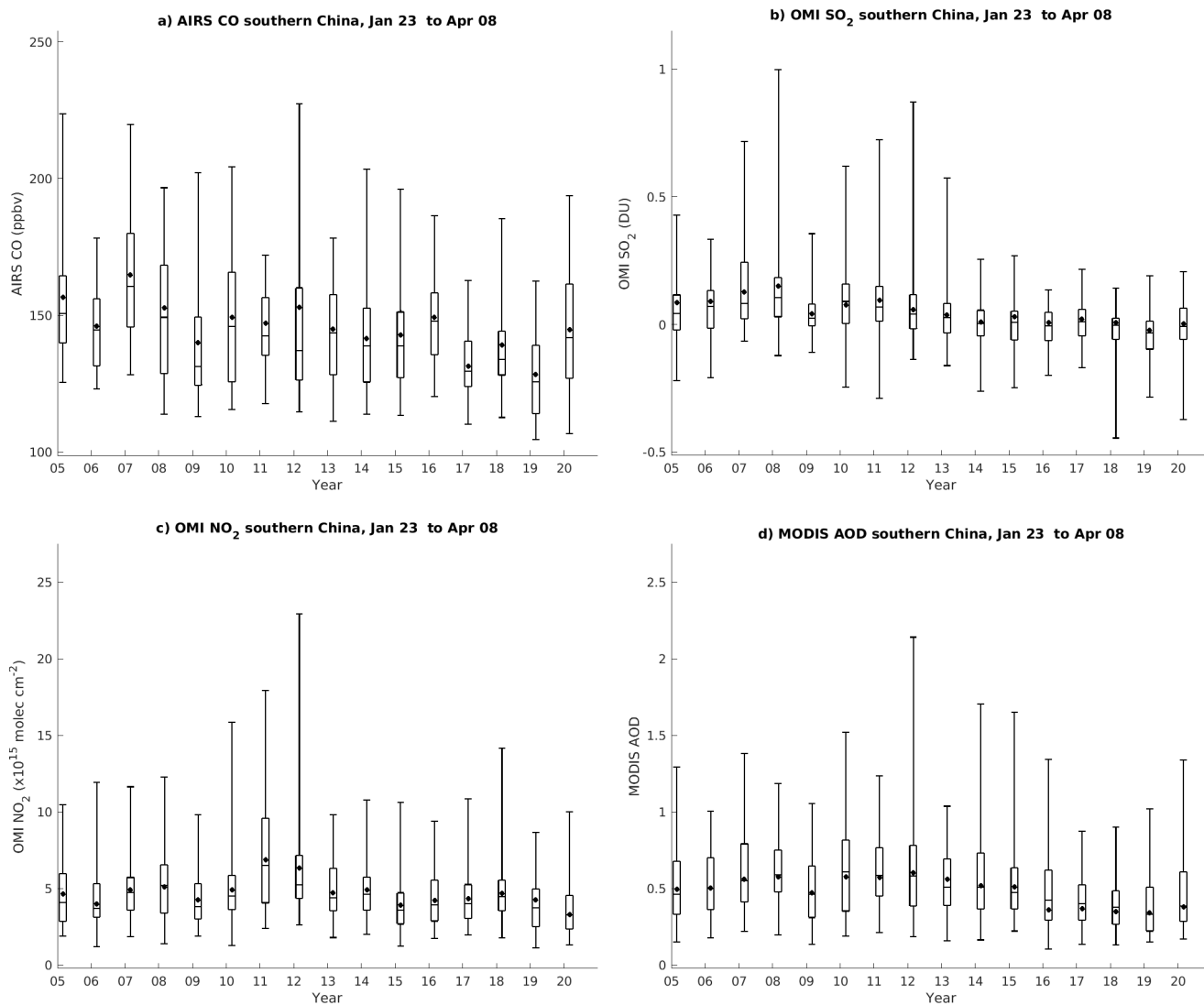
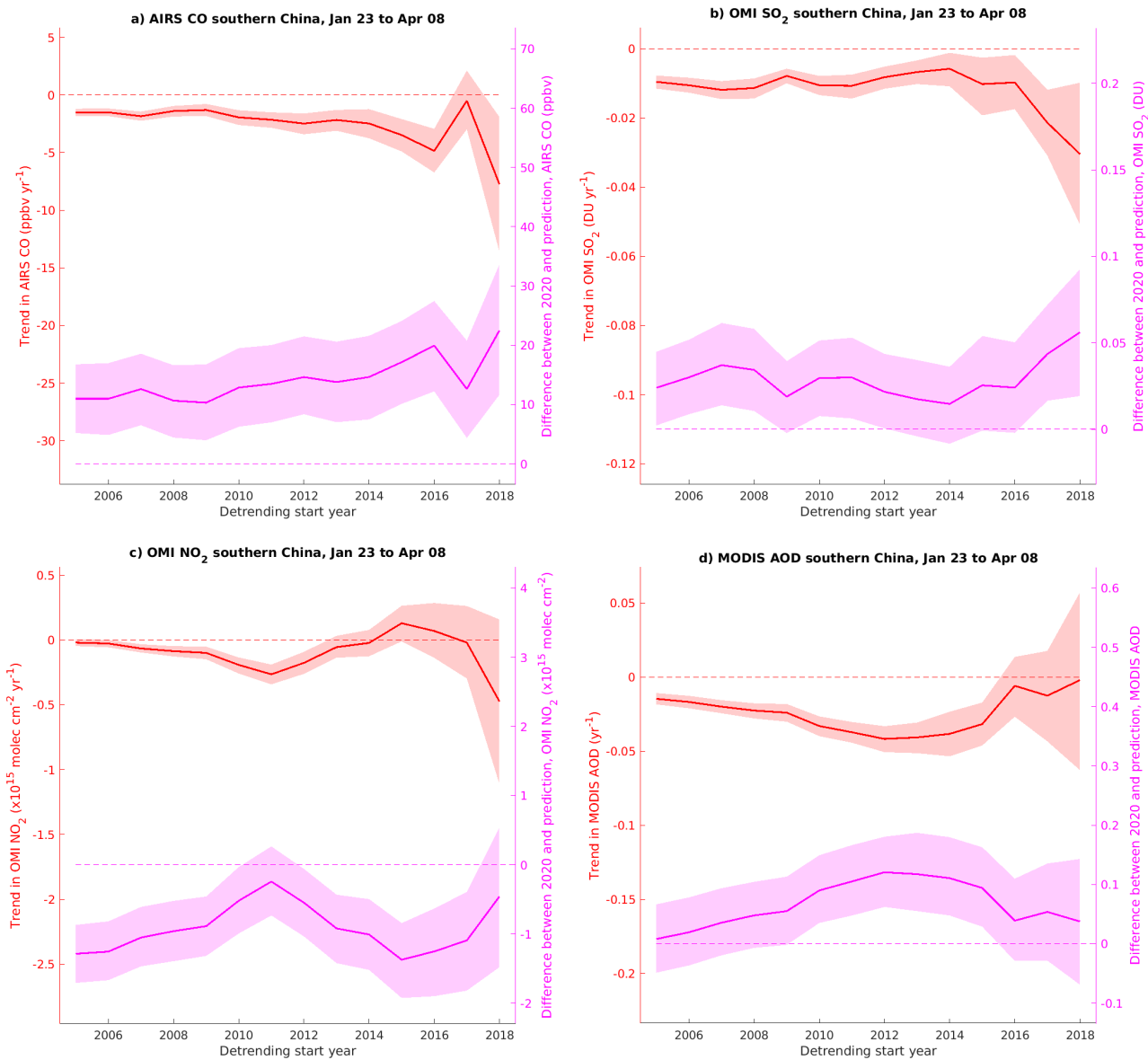


Figure 7. Same as Figure 5 but for southern China.



690 **Figure 8.** Same as Figure 6, but for southern China.